Metal–metal interactions in dinuclear ruthenium complexes incorporating "stepped-parallel" bridging ligands: synthesis, stereochemistry and intervalence charge transfer†

Deanna M. D'Alessandro and F. Richard Keene*

Received (in Durham, UK) 5th October 2005, Accepted 8th December 2005
First published as an Advance Article on the web 5th January 2006
DOI: 10.1039/b514111g

The synthesis and separation of the diastereoisomeric forms of the complexes $[\{Ru(bpy)_2\}_2(\mu\text{-BL})]^{4+}$ based on the series of "stepped-parallel" bridging ligands 2,5-bis(2-pyridyl)pyrazine (2,5-dpp), dipyrido(2,3-a;2′,3′-h)phenazine (dpop) and azobis(2-pyridine) (apy) are reported. Electrochemical and intervalence charge transfer (IVCT) studies on the complexes reveal a high degree of metal–metal interaction, consistent with a negligible solvent dependence of the IVCT parameters in each case. The results support a Class II–III classification for the systems.

Introduction

Experimental studies of IVCT in dinuclear mixed-valence complexes have provided crucial insights into the fundamental factors that govern electronic delocalisation and the barriers to electron transfer, through the seminal theoretical formalism pioneered by Hush.[1,2] To date, these factors have been probed predominantly by the variation of "global" features of the complexes, such as the identity and coordination environments of the constituent metal centres, or through variations in the macroscopic features of the medium such as the solvent, anions and temperature.[3–7] In many cases, the theoretical implications of the results have been confounded by ion-pairing and specific solvation effects, and ambiguities in the geometries of the complexes due to a lack of structural rigidity. In addition, electron transfer studies on dinuclear polypyridyl complexes of ruthenium and osmium have often neglected the inherent stereochemical complexities.

Keene and co-workers reported the first examples of differences in the photophysical, electrochemical and spectral properties of the stereoisomers in mono-, di- and trinuclear systems.[8–11] Recently, differences in the characteristics of the intervalence charge transfer properties of the diastereoisomers of dinuclear complexes as a function of solvent,[12] temperature, anions, and stereochemically-induced structural distortions[13,14] have provided detailed insights into the factors which govern the barriers to electron transfer at the molecular level. Within the semi-classical formalism for IVCT, the stereochemical effects are reflected in the inner- and outer-sphere Franck–Condon reorganisational contributions to the electron transfer barrier (λ_i and λ_o, respectively), the redox asymmetry factor (ΔE_0) and the spin–orbit coupling contribution ($\Delta E'$), as expressed in eqn (1).[1,2]

$$\nu_{max} = \lambda_i + \lambda_o + \Delta E_0 + \Delta E' \quad (1)$$

As shown in Fig. 1, the *meso* and *rac* diastereoisomers of symmetrical dinuclear complexes ($\Delta E_0 = 0$) such as $[\{Ru(bpy)_2\}_2(\mu\text{-}2,5\text{-dpp})]^{4+}$ {bpy = 2,2′-bipyridine; 2,5-dpp = 2,5-bis(2-pyridyl)pyrazine} differ only in terms of the relative orientations of the terminal ligands above and below the plane of the bridging ligand.[15,16] When the relationship between the axes of the "bites" of the two coordination sites of the bridging ligand are linear (*e.g.* bpm = 2,2′-bipyrimidine) or stepped-parallel (*e.g.* 2,5-dpp), the terminal ligands "above" and "below" the plane of the bridge are approximately parallel in the *rac* ($\Delta\Delta/\Lambda\Lambda$) form and orthogonal in the *meso* ($\Lambda\Delta$) diastereoisomer (Fig. 2). However, when the "bites" are angular (*e.g.* ppz = 4,7-phenanthrolino-5,6:5′,6′-pyrazine), this description is reversed.

The variation in the dimensionality of the clefts between the diastereoisomeric forms of the same complex provides a subtle and systematic probe for spatially-directed solvent and anion contributions to the electron transfer barrier. Previous investigations in our laboratory have elucidated the influences of stereochemically-directed interactions in ruthenium and osmium systems of the type $[\{M(bpy)_2\}_2(\mu\text{-BL})]^{5+}$ {BL = bridging ligand}, incorporating a broad series of linear[12] and angular[13,14,17,18] bridging ligands. The present investigation extends these studies to examine the modification of solvent reorganisational contributions in the diastereoisomers of complexes incorporating the stepped-parallel bridging ligands shown in Fig. 3.

The redox and spectral properties for the diastereoisomeric forms of $[\{Ru(bpy)_2\}_2(\mu\text{-BL})]^{4+}$ (BL = apy[8]) and for diastereoisomeric mixtures of $[\{Ru(bpy)_2\}_2(\mu\text{-BL})]^{4+}$ (BL = 2,5-dpp and dpop[19–25]) have been reported previously. However, their IVCT properties have received limited attention.[13,26,27] The bridging ligands possess unoccupied low-lying π* orbitals and mediate electron transfer between the metal centres *via* a superexchange-assisted electron transfer mechanism.[22] The subtle variations between the electronic characteristics of the

School of Pharmacy and Molecular Sciences, James Cook University, Townsville, Queensland 4811, Australia. E-mail: Richard.Keene@jcu.edu.au; Fax: +61-(0)7-4781-6078

† Electronic supplementary information (ESI) available: Redox potentials for reductions and IVCT transition data for the diastereoisomers of $[\{Ru(bpy)_2\}_2(\mu\text{-BL})]^{4+}$ and views of the diastereoisomers of $[\{Ru(bpy)_2\}_2(\mu\text{-bpm})]^{4+}$. See DOI: 10.1039/b514111g

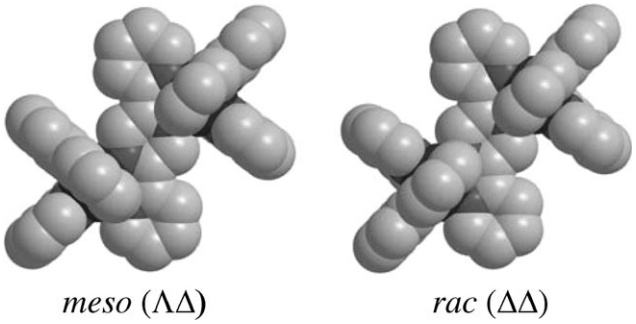

Fig. 1 Chem3D™ representations[52] (view from above the plane of the bridging ligand) of the *meso* (ΛΔ) and *rac* (ΔΔ) diastereoisomers of $[\{Ru(bpy)_2\}_2(\mu\text{-}2,5\text{-}dpp)]^{4+}$ showing the different dimensions of the clefts "above" and "below" the plane of the bridging ligand.

series of ligands, and the distance between the metal centres which are coordinated at the two bidentate sites in each case, provide detailed insights into the influence of the degree of electronic delocalisation (H_{ab}) on the IVCT properties.

Experimental

Materials

Potassium hexafluorophosphate (KPF_6; Aldrich, 98%), ammonium hexafluorophosphate (NH_4PF_6; Aldrich), ethylene glycol (Ajax 95%), sodium toluene-4-sulfonate (Aldrich, 98%), DOWEX® 1 × 8, 50–100 mesh Cl^- anion exchange resin (Aldrich), Celite (Aldrich) and laboratory reagent solvents were used as received. Tetra-*n*-butylammonium hexafluorophosphate ($[(n\text{-}C_4H_9)_4N]PF_6$; Fluka, 99+%) was dried

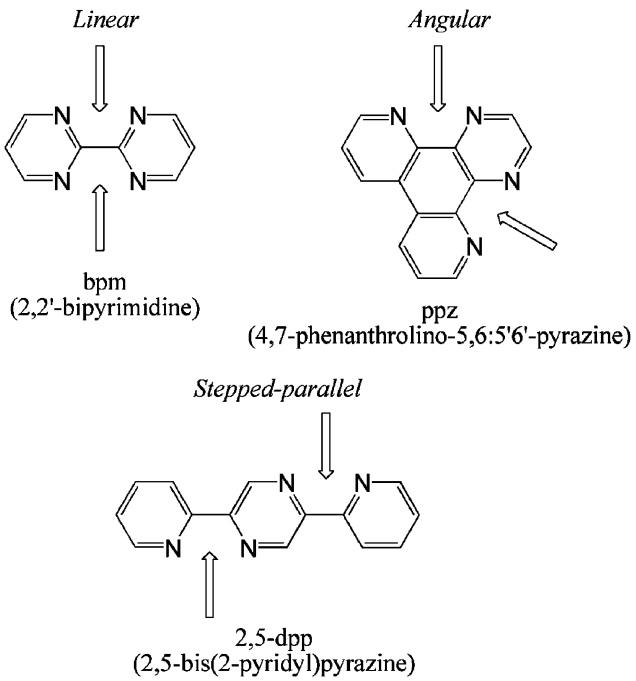

Fig. 2 Examples of bridging di-bidentate ligands commonly used in the construction of polymetallic assemblies. The bridging ligands may be categorised as linear, angular or stepped-parallel based on the relative disposition of the bidentate coordination sites.

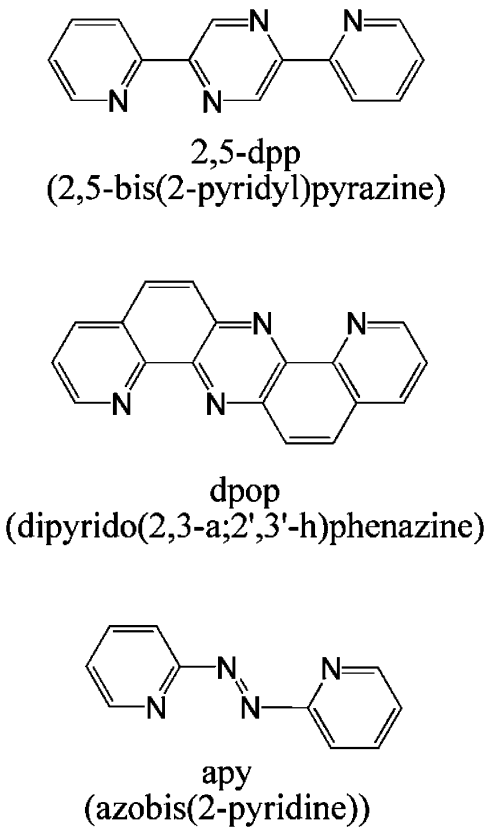

Fig. 3 "Stepped-parallel" polypyridyl bridging ligands employed in the present study.

in vacuo at 60 °C prior to use and ferrocene (Fc; BDH) was purified by sublimation prior to use. SP Sephadex C-25 (Amersham Pharmacia Biotech) and silica gel (200–400 mesh, 60 Å, Aldrich) were employed for the chromatographic separation and purification of ruthenium complexes.[15] Prior to use, acetonitrile (CH_3CN; Aldrich, 99.9+%) and propionitrile (PN; Aldrich) were distilled over CaH_2, while acetone (BDH, HPLC grade) was distilled over K_2CO_3 and dichloromethane over $CaCl_2$. *n*-Butyronitrile (BN; Aldrich, 99+%), isobutyronitrile (^{i}BN; Aldrich), and benzonitrile (BzN; Aldrich) were used as received. $[(n\text{-}C_4H_9)_4N]\{B(C_6F_5)_4\}$[28] was prepared by metathesis from $Li\{B(C_6F_5)_4\} \cdot Et_2O$ as described previously.[12] 2,5-Bis(2-pyridyl)pyrazine (2,5-dpp) was supplied by Dr Bradley Patterson.[29] Ferrocene (Fc; BDH) was purified by sublimation before use.

General

1D and 2D ^1H NMR spectra were collected on a Varian Mercury 300 MHz spectrometer. ^1H NMR chemical shifts for all complexes are reported relative to 99.9% d_3-acetonitrile $\{CD_3CN$; Cambridge Isotope Laboratories (CIL)$\}$ at $\delta = 1.93$ ppm. ^1H NMR assignments were performed with the assistance of COSY experiments to identify each pyridine ring system. Elemental microanalyses were performed at the Microanalytical Unit in the Research School of Chemistry, Australian National University. For selected complexes, an allowance for hydration was necessary to account for analysis figures within the acceptable limits (±0.4%).

Electrochemistry

Electrochemical measurements were performed under argon using a Bioanalytical Systems (BAS) 100A electrochemical analyser. Cyclic (CV) and differential pulse (DPV) voltammograms were recorded in a standard three-electrode cell using a glassy carbon or platinum button working electrode, a platinum wire auxiliary electrode and an Ag/AgCl reference electrode {0.1 M $[(n\text{-}C_4H_9)_4N]PF_6$ in CH_3CN}. Ferrocene was added as an internal standard on completion of each experiment {the ferrocene/ferrocenium couple (Fe^+/Fe^0) occurred at +550 mV *versus* Ag/AgCl). Solutions contained 0.1 M $[(n\text{-}C_4H_9)_4N]PF_6$ as electrolyte. Cyclic voltammetry was performed with a sweep rate of 100 mV s^{-1}; differential pulse voltammetry was conducted with a sweep rate of 4 mV s^{-1} and a pulse amplitude, width and period of 50 mV, 60 ms and 1 s, respectively. All potentials are reported ±3 mV.

UV/Vis/NIR spectroelectrochemistry

UV/Vis/NIR spectroelectrochemistry was performed using a CARY 5E spectrophotometer interfaced to Varian WinUV software.[53] The absorption spectra of the electrogenerated mixed-valence species were obtained *in situ* by the use of a cryostatted optically semi-transparent thin-layer electrosynthetic (OSTLE) cell.[30] An account of the procedure employed in the spectroelectrochemical measurements has been detailed previously.[31] Solutions for the spectroelectrochemical experiments contained 0.02 M $[(n\text{-}C_4H_9)_4N]\{B(C_6F_5)_4\}$ supporting electrolyte in CH_3CN and the complex (*ca.* 0.4×10^{-3} M). The temperature was stabilised to ±0.3 °C prior to commencing electrolysis. The dinuclear systems required approximately 6 h for data collection at −35 °C.

The analysis and spectral deconvolution of the data were performed as described in a previous report.[14] The IVCT spectra were scaled as $\int\varepsilon(\nu)/\nu\ d\nu$ [1,32] and deconvolution of the NIR transitions was performed using the curve-fitting subroutine implemented within the GRAMS32 commercial software package, as described previously.[31] Based on the reproducibility of the parameters obtained from the deconvolutions, the uncertainties in the energies (ν_{max} in cm^{-1}), intensities $\{(\varepsilon/\nu)_{max}$ in $M^{-1}\}$ and bandwidths ($\Delta\nu_{\frac{1}{2}}$ in cm^{-1}) were estimated as ±10 cm^{-1}, ±0.001 M^{-1} and ±10 cm^{-1}, respectively.

For asymmetrically-shaped IVCT bands, an examination of the moments of the band are required, rather than the experimentally-observed quantities $\{\nu_{max}$, $\Delta\nu_{\frac{1}{2}}$ and $(\varepsilon/\nu)_{max}\}$. The first-order moment (M_1) defines the average energy of the absorption manifold and is given by eqn (2).[1] $f(\nu)$ is the lineshape function of the reduced absorption spectrum {(ε/ν) *vs.* ν}. The denominator represents the area under the band of the reduced absorption spectrum, *i.e.* the zeroth-moment, M_0 {eqn (3)}. The transition moment ($|\mu_{12}|$ in eÅ) is defined as 0.0206 Å $\times$ $M_0^{\frac{1}{2}}$.

$$M_1 = \frac{1}{M_0}\int_{\nu_1}^{\nu_2} \nu f(\nu)\mathrm{d}\nu \qquad (2)$$

$$M_0 = \frac{1}{M_0}\int_{\nu_1}^{\nu_2} f(\nu)\mathrm{d}\nu \qquad (3)$$

Synthesis of dinuclear complexes, and separation of diastereoisomers

A detailed account of the microwave techniques and column chromatographic procedures employed for the separation and purification of the diastereoisomers has been reported previously.[33] The synthesis of $[Ru(bpy)_2Cl_2]\cdot 2H_2O$,[34] and the synthesis and diastereoisomer separation of $[\{Ru(bpy)_2\}_2(\mu\text{-apy})](PF_6)_4$ were performed according to the literature procedures.[8] $[\{Ru(bpy)_2\}_2(\mu\text{-dpop})](PF_6)_4$ was supplied by Prof. Tom Meyer and Dr Dana Dattelbaum (Los Alamos National Laboratory).

$[\{Ru(bpy)_2\}_2(\mu\text{-2,5-dpp})](PF_6)_4$. The complex was synthesised by an adaptation of the literature procedure.[35] A suspension of 2,5-dpp (18.3 mg, 0.0873 mmol) in ethylene glycol (3 cm^3) was heated in a modified microwave oven on medium high power for 20 s to complete dissolution. *cis*-$[Ru(bpy)_2Cl_2]\cdot 2H_2O$ (100 mg, 0.192 mmol) was added and the mixture heated at reflux for a further 8 min on high power, during which time the solution attained a dark purple colouration. The mixture was diluted in water (*ca.* 50 cm^3) and the dinuclear product was separated from the crude mixture *via* a gradient elution procedure using aqueous 0.1–0.5 M NaCl as the eluent. A band of mononuclear material eluted first (0.2 M NaCl) followed by the desired dark purple product (0.4 M NaCl) which was precipitated as the PF_6^- salt by addition of a saturated solution of aqueous KPF_6. The solid was isolated by vacuum filtration and washed with diethyl ether (3 × 10 cm^3). Yield: 130 mg (92%). Anal. Calcd for $C_{52}H_{42}F_{24}N_{12}P_4Ru_2$: C, 38.6; H, 2.62; N, 10.4%. Found: C, 38.4; H, 2.45; N, 10.3%.

Separation of the diastereoisomers was achieved by cation-exchange chromatography on SP Sephadex C-25 support (dimensions 96 cm length × 1.6 cm diameter). The complex (*ca.* 100 mg) was loaded onto the column in aqueous solution (as the Cl^- form, obtained by stirring an aqueous suspension of the complex with DOWEX® anion exchange resin) and eluted with 0.25 M sodium toluene-4-sulfonate solution.[33] Using a recycling technique described elsewhere,[33] the diastereoisomers separated after passing through an effective column length of 2 m. The two bands were collected, saturated aqueous KPF_6 solution added and the products extracted with dichloromethane. The organic extracts were dried with anhydrous Na_2SO_4 and the solvent removed by rotary evaporation.

Rigorous purification methods were employed prior to characterisation and physical measurements due to the potentially strong associations between the complex cations and the anions present in the eluents employed in the chromatographic separations.[33,36] Each product was dissolved in a minimum volume of acetone and loaded onto a short column of silica gel (dimensions 3 × 2.5 cm), washed with acetone, water and acetone and eluted with acetone containing 5% NH_4PF_6. Addition of water and removal of the acetone under reduced pressure afforded dark purple solids which were collected by filtration through Celite and washed with diethyl ether (3 × 5 cm^3). In each case the precipitate was washed off the Celite into a test tube with acetone (*ca.* 2 cm^3), evaporated under a stream of dry N_2 and dried *in vacuo* for 3 h at 50 °C. Bands 1

and 2 were determined to be the *rac* and *meso* diastereoisomers, respectively, as established by NMR characterisation and comparison with the ^{1}H NMR spectra for [{Ru(phen)$_2$}$_2$(μ-2,5-dpp)](PF$_6$)$_4$ (phen = 1,10-phenanthroline) reported by Hua.[35] ^{1}H NMR (δ ppm; CD_3CN): (**Band 1**; *rac*) 7.31 (H5b, 2H, J = 8, 5 Hz, dd), 7.46 (H5b, H5c, 4H, J = 8, 5 Hz, dd), 7.51 (H6d, H6b, 4H, J = 5, 1.5 Hz, dd), 7.59 (H5a, H4 2,5-dpp, 4H, J = 8, 5 Hz, dd), 7.77 (H6c, 2H, J = 5, 1.5 Hz, dd), 7.83 (H6a, 2H, J = 5, 1.5 Hz, dd), 7.90 (H6 2,5-dpp, 2H, J = 8 Hz, d), 7.98 (H4d, 2H, J = 8, 8 Hz, dd), 8.03 (H6b, 2H, J = 5, 1.5 Hz, dd), 8.10 (H4c, 2H, J = 8, 8 Hz, dd), 8.13 (H4a, 2H, J = 8, 8 Hz, dd), 8.17 (H4, 2H, J = 8, 8 Hz, dd), 8.20 (H4, 2H, J = 8, 8 Hz, dd), 8.38 (H7/H14 2,5-dpp, 2H, s), 8.54 (H3d, 2H, J = 8, 1.5 Hz, dd), 8.56 (H3b, H3c, H3a, 6H, J = 8 Hz, d); (**Band 2**; *meso*) 7.19 (H4 2,5-dpp, 2H, J = 8, 5 Hz, dd), 7.48 (H5d, H5b, 4H, J = 8, 5 Hz, dd), 7.50 (H5c, 2H, J = 8, 5 Hz, dd), 7.56 (H3 2,5-dpp, H6d, 4H, J = 5, 1.5 Hz, dd), 7.65 (H6c, H6a, 4H, J = 5, 1.5 Hz, dd), 7.76 (H6d, H6b, 4H, J = 5, 1.5 Hz, dd), 7.90 (H4 2,5-dpp, 2H), 7.96 (H4d, 2H, J = 8, 8 Hz, dd), 8.06 (H4b, 2H, J = 8, 8 Hz, dd), 8.11 (H4c, 2H, J = 8, 8 Hz, dd), 8.17 (H5 2,5-dpp, 2H, J = 8, 8 Hz, dd), 8.21 (H4a, 2H, J = 8, 8 Hz, dd), 8.42 (H7/H14 2,5-dpp, 2H, s), 8.50 (H6/13 2,5-dpp, 2H, J = 8, 1.5 Hz, dd), 8.54 (H3d, 2H, J = 8, 1.5 Hz, dd), 8.56 (H3b, 2H, J = 8, 1.5 Hz, dd), 8.59 (H3c, 2H, J = 8, 1.5 Hz, dd).

[{Ru(bpy)$_2$}$_2$(μ-dpop)](PF$_6$)$_4$. The separation and purification of the diastereoisomeric forms were achieved as described previously, using 0.25 M sodium toluene-4-sulfonate solution as the eluent. ^{1}H NMR (δ ppm; CD_3CN): (**Band 1**; *rac*) 6.97 (H5d, 2H, J = 8, 5 Hz, dd), 7.21 (H6d, 2H, J = 5, 1.5 Hz, dd), 7.28 (H5b, 2H, J = 5, 1.5 Hz, dd), 7.29 (H6b, 2H, J = 5, 1.5 Hz, dd), 7.45 (H6/13 dpop, 2H, J = 8 Hz, d), 7.51 (H5a, 2H, J = 5, 1.5 Hz, dd), 7.57 (H5c, 2H, J = 5, 1.5 Hz, dd), 7.66 (H6a, 2H, J = 5, 1.5 Hz, dd), 7.86 (H7/14 dpop, 2H, J = 10, 8 Hz, dd), 7.93 (H6c, 2H, J = 5, 1.5 Hz, dd), 8.05 (H4d, 2H, J = 8, 8 Hz, dd), 8.08 (H4c, 2H, J = 8, 8 Hz, dd), 8.14–8.20 (2H, m), 8.23 (H4a, 2H, J = 8, 8 Hz, dd), 8.49 (H3a, 2H, J = 8, 1.5 Hz, dd), 8.51 (H3c, 2H, J = 8, 1.5 Hz, dd), 8.57 (H3d, 2H, J = 8, 1.5 Hz, dd), 8.61 (H3a, 2H, J = 8, 1.5 Hz, dd); (**Band 2**; *meso*) 6.51 (H6b, 2H, J = 5, 1.5 Hz, dd), 6.77 (H5b, 2H, J = 8, 5 Hz, dd), 7.31 (H5d, 2H, J = 8, 5 Hz, dd), 7.43 (H5c, 2H, J = 8, 5 Hz, dd), 7.59 (H6/13 dpop, 2H, J = 8 Hz, d), 7.62 (H6c, 2H, J = 5, 1.5 Hz, dd), 7.65 (H6a, 2H, J = 5, 1.5 Hz, dd), 7.82 (H7/14 dpop, 2H, J = 10, 8 Hz, dd), 7.82 (H5a, 2H, J = 8, 5 Hz, dd), 8.04 (H6d, 2H, J = 5, 1.5 Hz, dd), 8.10 (H4b, 2H, J = 8, 8 Hz, dd), 8.11 (H4a, 2H, J = 8, 8 Hz, dd), 8.14–8.22 (10H, m), 8.40 (H3a, 2H, J = 8, 1.5 Hz, dd), 8.62 (H3b, 2H, J = 8, 1.5 Hz, dd), 8.68 (H3b, H3c, 4H, J = 8, 1.5 Hz, dd).

Results and discussion

Diastereoisomer synthesis, separation and structural characterisation

The complexes [{Ru(bpy)$_2$}$_2$(μ-BL)]$^{4+}$ {BL = 2,5-dpp, dpop} were synthesised by the reaction of 2.2 equivalents of *cis*-[Ru(bpy)$_2$Cl$_2$]·2H$_2$O with the bridging ligand in ethylene glycol, using the microwave-assisted methodology which is well established for the synthesis of a range of dinuclear polypyridyl complexes of ruthenium.[10,13,26,27,33] This technique produced equivalent or increased reaction yields of the dinuclear species compared with previously reported thermal methods for the synthesis of [{Ru(bpy)$_2$}$_2$(μ-2,5-dpp)]$^{4+}$.[37] However, there was a significant reduction in the reaction times (typically from 45 min for the osmium complexes and 2–24 h for the ruthenium complexes under the thermal refluxing procedure) to *ca.* 10 min under microwave-assisted conditions.

The separation of the diastereoisomeric forms of the dinuclear complexes was achieved by cation-exchange chromatography using SP Sephadex C-25 as the support with aqueous solutions of sodium toluene-4-sulfonate as the eluent. The Band 1 and 2 eluates were determined to be the *rac* and *meso* diastereoisomers, respectively, which contrasts the elution order which has been observed previously for complexes incorporating linear and angular bridging ligands such as those shown in Fig. 2.

^{1}H NMR studies

The assignments of the ^{1}H NMR spectra for the diastereoisomers of [{Ru(bpy)$_2$}$_2$(μ-apy)]$^{4+}$ have been reported previously.[8] The ^{1}H numbering schemes for the diastereoisomers of [{Ru(bpy)$_2$}$_2$(μ-dpop)]$^{4+}$ are shown in Fig. 4 and the

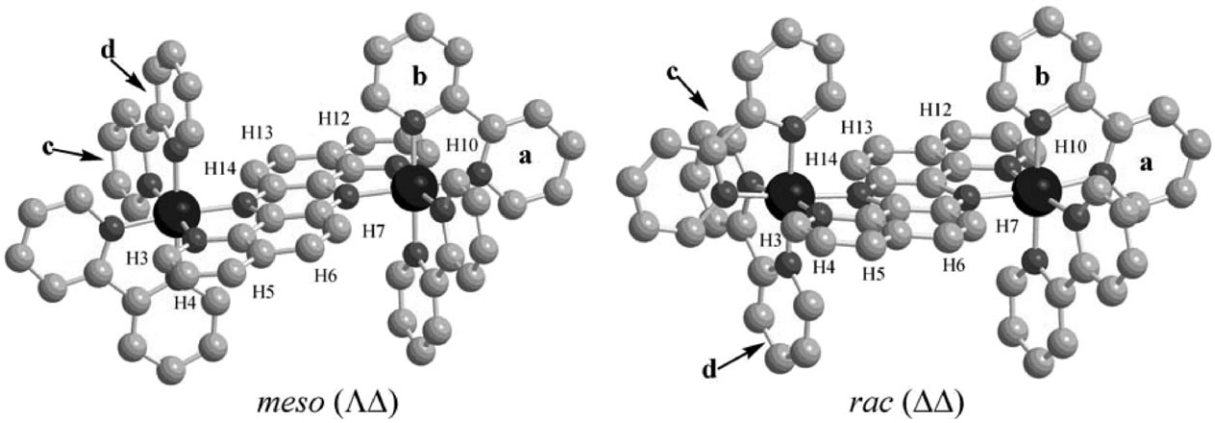

Fig. 4 Chem3D™ representations[52] of *meso*-(ΛΔ)- and *rac*-(ΔΔ)-[{Ru(bpy)$_2$}$_2$(μ-dpop)]$^{4+}$ with NMR labelling scheme for the bpy ligands, and numbering scheme for the dpop protons. Hydrogen atoms are omitted for clarity.

assignments of the spectra were performed with the assistance of ^{1}H COSY spectra and by comparison with the previously reported spectral assignments for $[\{Ru(phen)_2\}_2(\mu\text{-}2,5\text{-dpp})]^{4+}$.[35] The coordinated bpy ligands exhibited the expected coupling constant values[38] {$J_{3,4}$ = 8 Hz, $J_{3,5}$ = 1.5 Hz, $J_{4,5}$ = 8 Hz, $J_{4,6}$ = 1.5 Hz and $J_{5,6}$ = 5 Hz} and coupling patterns based on the symmetry requirements of the complexes.

The *meso* and *rac* diastereoisomers of $[\{Ru(bpy)_2\}_2(\mu\text{-BL})]^{4+}$ {BL = 2,5-dpp, dpop} possess C_i and C_2 point group symmetries, respectively. Four different "pyridyl" environments are distinguished for the two non-equivalent bpy ligands (giving rise to 16 non-equivalent bpy resonances). In addition, one set of four coupled protons and one singlet resonance arise from the bridging ligand 2,5-dpp, while five non-equivalent proton resonances arise from the dpop ligand.

The H5 and H6 protons of the pyridyl rings situated over the plane of the bridging ligand experience the most pronounced chemical shift differences between the diastereoisomeric forms of a given complex. In the *meso* diastereoisomer, *ring b* is oriented over the plane of BL and the bpy ligand across the bridge such that the H5/H6 protons of this ring experience increased diamagnetic anisotropic effects (and hence occur slightly upfield) relative to the H5/H6 protons of *ring d*. In the *rac* diastereoisomer, the H6 proton of *ring b* is situated over the plane of BL and in the deshielding cone of bpy *ring b* across the bridge. This proton experiences a slightly decreased shielding influence relative to the H6 proton of *ring b* in the *meso* diastereoisomer. The remaining spectral assignments were performed with the assistance of ^{1}H COSY spectra.

Electrochemical and UV/Vis/NIR spectral characterisation

The redox potentials for the E_{ox1} ([5+/4+]; *i.e.* Ru^{III}–Ru^{II}/Ru^{II}–Ru^{II}) and E_{ox2} ([6+/5+]; *i.e.* Ru^{III}–Ru^{III}/Ru^{III}–Ru^{II}) couples for *meso*- and *rac*-$[\{Ru(bpy)_2\}_2(\mu\text{-BL})]^{4+}$ {BL = 2,5-dpp, dpop} were investigated by cyclic and differential pulse voltammetry in acetonitrile containing 0.1 M $[(n\text{-}C_4H_9)_4N]PF_6$, and are reported in Table 1. The redox potentials for the ligand-based reductions are reported in Table S1 (ESI†). ΔE_{ox} defines the potential difference between the [6+/5+] and [5+/4+] couples. The electrochemical and UV/Vis characteristics of *meso*- and *rac*-$[\{Ru(bpy)_2\}_2(\mu\text{-apy})]^{n+}$ (n = 4, 5, 6)[8] have been reported previously.

Table 1 Electrochemical data (in mV relative to the Fc^+/Fc^0 couple) and comproportionation constants[a] (K_c) for $[\{Ru(bpy)_2\}_2(\mu\text{-BL})]^{4+}$ in 0.1 M $[(n\text{-}C_4H_9)_4N]PF_6$–$CH_3CN$.[b]

BL	Diastereoisomer	K_c	ΔE_{ox}	E_{ox2}	E_{ox1}
2,5-dpp	*meso*	4.31×10^3	215	1185	970
	rac	3.55×10^3	210	1186	976
dpop	*meso*	3.15×10^3	207	1279	1072
	rac	2.40×10^3	200	1276	1076
apy[c]	*meso*	1.92×10^8	490	1945	1455
	rac	2.83×10^8	500	1965	1465

[a] K_c values are given by $K_c = \exp(\Delta E_{ox}F/RT)$ where F/RT = 38.92 V^{-1} at 298 K.[3] [b] $\Delta E_{ox} = E_{ox2} - E_{ox1}$. Potentials are quoted ±3 mV. [c] Potentials measured in 0.1 M $[(n\text{-}C_4H_9)_4N]ClO_4$–$CH_3CN$.[8]

The dinuclear systems are each characterised by two reversible one-electron redox processes corresponding to successive oxidation of the metal centres, in addition to multiple reversible ligand-based reductions in the cathodic region. In the cathodic region, the first two processes are assigned to the successive one-electron reductions of the bridging ligands ($BL^{0/-}$ and $BL^{-/2-}$), consistent with the stronger π-acceptor nature of the bridging relative to the terminal bpy ligands.[8,19–25,39,40] The subsequent four one-electron processes correspond to successive reduction of the terminal bpy ligands. The shift of E_{red1} and E_{red2} towards increasingly positive potentials as the bridging ligand is varied through the series 2,5-dpp, dpop and apy is consistent with the stabilisation of the π*(BL) LUMOs.

Measurable differences in the ΔE_{ox} values are evident between the different complexes and between the diastereoisomeric forms of the same complex. The magnitudes of ΔE_{ox} and the comproportionation constant[3] (K_c) increase as BL is varied through the series dpop, 2,5-dpp and apy. However, these differences cannot be solely ascribed to variations in the extent of electronic delocalisation due to structural factors, as the magnitude of ΔE_{ox} also reflects contributions from ion-pairing interactions,[41] solvation energies and statistical factors.[42,43]

IVCT solvatochromism measurements for the diastereoisomeric forms of $[\{Ru(bpy)_2\}_2(\mu\text{-BL})]^{5+}$ {BL = 2,5-dpp, dpop and apy} were performed in the homologous series of nitrile solvents acetonitrile (CH_3CN or AN), propionitrile (PN), *n*-butyronitrile (BN), isobutyronitrile (^{i}BN) and benzonitrile (BzN) containing 0.02 M $[(n\text{-}C_4H_9)_4N]\{B(C_6F_5)_4\}$[28] electrolyte. The UV/Vis/NIR spectral characteristics of the +4 (unoxidised) and +5 (mixed-valence) states of the complexes are reported in Table 2, and the spectra in *n*-butyronitrile solution are shown in Fig. 5. The spectroelectrochemical oxidation of the 2,5-dpp- and dpop-bridged systems was performed at +25 °C, while the apy-bridged diastereoisomers were unstable at room temperature and required low temperature spectroelectrochemical generation at −35 °C (*i.e.* below the freezing point of BzN).

The spectra are characterised by a combination of overlapping $d\pi(Ru^{II}) \rightarrow \pi^*$(BL, bpy) singlet metal-to-ligand (^{1}MLCT) transitions. The lowest energy absorption band shifts to the red as BL is varied through the series 2,5-dpp, dpop and apy, consistent with the increasing stabilisation of the π*(BL) orbitals. The lowest energy absorption bands for the series of complexes are assigned as $d\pi(Ru) \rightarrow \pi^*$(BL) MLCT transitions, and decreased in intensity on one-electron oxidation to the +5 state.

Intervalence charge transfer

The IVCT properties for the diastereoisomers of $[\{Ru(bpy)_2\}_2(\mu\text{-apy})]^{4+}$ in 0.1 M $[(n\text{-}C_4H_9)_4N]ClO_4$–$CH_3CN$ electrolyte have been discussed previously.[8] In the present study, IVCT solvatochromism measurements on the diastereoisomers were performed at −35 °C in 0.02 M $[(n\text{-}C_4H_9)_4N]\{B(C_6F_5)_4\}$ electrolyte,[28] containing a uniform low concentration of the given diastereoisomer (0.40×10^{-3} M) to eliminate ion-pairing artefacts which are known to influence the IVCT characteristics.[14] The mixed-valence species exhibit IVCT

Table 2 UV/Vis/NIR spectral data for the stepped-parallel dinuclear complexes $[\{Ru(bpy)_2\}_2(\mu\text{-BL})]^{n+}$ in 0.02 M $[(n\text{-}C_4H_9)_4N]\{B(C_6F_5)_4\}$–$CH_3CN$ at +25 °C for BL = 2,5-dpp, dpop and −35 °C for BL = apy. The parameters of the IVCT bands are indicated in bold type

BL		2,5-dpp		dpop		apy	
Diastereoisomer	*n*	ν ±10 (cm^{-1})	(ε/ν) ±0.001 (M^{-1})	ν ±10 (cm^{-1})	(ε/ν) ±0.001 (M^{-1})	ν ±10 (cm^{-1})	(ε/ν) ±0.001 (M^{-1})
meso	4	17105	0.939	15025	1.899	12940	2.083
		23180	0.735	24030	0.768	25340	0.840
		28160	1.070	26920	0.906		
	5	**5460**	**0.356**	**5228**	**0.315**	**6840**	**0.243**
		16835	0.616	14940	1.127	12800	0.863
		23700	0.325	26000	0.775	14480	0.860
		27470	0.953			24540	1.055
rac	4	17100	0.794	15120	1.803	12865	2.661
		23140	0.655	23890	0.736	25265	1.053
		28220	0.943	26930	0.890		
	5	**5416**	**0.428**	**5268**	**0.247**	**6850**	**0.143**
		16930	0.509	14980	1.088	12915	0.592
		23550	0.294	26100	0.724	14345	0.505
		27670	0.763			24735	0.738

bands in the region 4000–9000 cm^{-1} for $[\{Ru(bpy)_2\}_2(\mu\text{-BL})]^{5+}$ (BL = 2,5-dpp, dpop) and 6000–9000 cm^{-1} for $[\{Ru(bpy)_2\}_2(\mu\text{-apy})]^{5+}$, as shown in Fig. 6, and the results of the band maxima (ν_{max} in cm^{-1}), molar absorption coefficients $\{(\varepsilon/\nu)_{max}$ in $M^{-1}\}$, bandwidths ($\Delta\nu_{\frac{1}{2}}$ in cm^{-1}) in acetonitrile solution are summarised in Table 3. For all complexes, the bands are asymmetrically-shaped and narrower on the lower energy side. A moment analysis of the IVCT bands was pursued,[1,32] and the results for the second-order moment analysis are also presented in Table 3, where the zeroth- (M_0) and first-order (M_1) moments represent the band area and average band energy, respectively, and $|\mu_{12}|$ is the adiabatic transition moment. Since the IVCT bands are overlapped on the high energy side by the lowest energy MLCT transition for the apy-bridged diastereoisomers, accurate determinations of M_1 were not possible, and the $\Delta\nu_{\frac{1}{2}}$ values were obtained by fitting the low energy side of the IVCT manifold with a single Gaussian-shaped band. The electronic coupling parameters, H_{ab}, were determined from eqn (4),[44,45] where e is the unit electronic charge and r_{ab} was equated with the through-space geometrical distance between the metal centres[7] which was estimated as the geometric Ru···Ru distance of 6.9 Å for $[\{Ru(bpy)_2\}_2(\mu\text{-BL})]^{5+}$ {BL = 2,5-dpp, dpop} and 4.9 Å for $[\{Ru(bpy)_2\}_2(\mu\text{-apy})]^{5+}$ from molecular models.

$$H_{ab} = \frac{|\mu_{12}|}{er_{ab}}\nu_{max} \qquad (4)$$

A classical two-state analysis[46] of the IVCT transitions reveals that all the systems exhibit significant electronic delocalisation. On the basis of the narrow bandwidths compared with the comparison with the theoretical bandwidths ($\Delta\nu_{\frac{1}{2}}^{\circ} = [16RT\ln2(\lambda)]^{\frac{1}{2}}$, where $16RT\ln2 = 1836\ cm^{-1}$ at 238 K and 2562 cm^{-1} at 298 K) the systems lie close to the localised-to-delocalised transition. Due to the shorter inter-metal separation in the apy-bridged systems (*ca.* 4.9 Å) the IVCT process is facilitated by direct overlap of the Ru(dπ) orbitals,[19–21] in addition to superexchange interactions *via* the π-system of the bridging ligand.[22–25] These factors may explain the higher energy of the IVCT bands for the apy-bridged systems relative to the 2,5-dpp- and dpop-bridged complexes (in which the inter-metal separation is *ca.* 6.9 Å).

It must be noted that since electronic coupling decreases the *effective* electron transfer distance relative to the geometrical metal–metal separation {which is equated with r_{ab} in eqn (4)}, the H_{ab} values presented in Table 3 represent lower limits for the electronic coupling parameter.

IVCT solvatochromism

The IVCT parameters for the complexes in the series of nitrile solvents are reported in Tables 4–6. Fig. 7 presents an overlay of the solvent dependence of the IVCT band parameters ν_{max}, $\Delta\nu_{\frac{1}{2}}$ and M_1, and Table 7 summarises the results for the slopes and intercepts of the solvatochromism plots. The data reveal differences in the solvent dependencies of the IVCT parameters between the different complexes, and between the diastereoisomers of the same complex.

In accordance with the dielectric continuum model (5), ν_{max} should exhibit a linear dependence on $1/D_{op} - 1/D_s$, with slope $e^2(1/D_{op} - 1/D_s)$ and intercept $\lambda_i + \Delta E_0 + \Delta E'$.[1,2] The parameters a and d define the molecular radii and distance between the donor and acceptor, and D_s and D_{op} are the static and optical dielectric constants of the solvent, respectively.

$$\lambda_o = e^2\left(\frac{1}{a} - \frac{1}{d}\right)\left(\frac{1}{D_{op}} - \frac{1}{D_s}\right) \qquad (5)$$

In general, the IVCT parameters for the series of complexes exhibit a weak dependence on $1/D_{op} - 1/D_s$, as shown in Fig. 7, which is consistent with charge transfer transitions involving a minimal dipole moment change, a small residual barrier to intramolecular electron transfer, and the classification of the complexes as borderline localised-to-delocalised systems.[7] While the classification of mixed-valence systems is not straightforward and relies on observations from several experimental techniques with widely different time-scales,[7] the appearance of IVCT bands and their solvent dependence provides the most useful experimental criterion for

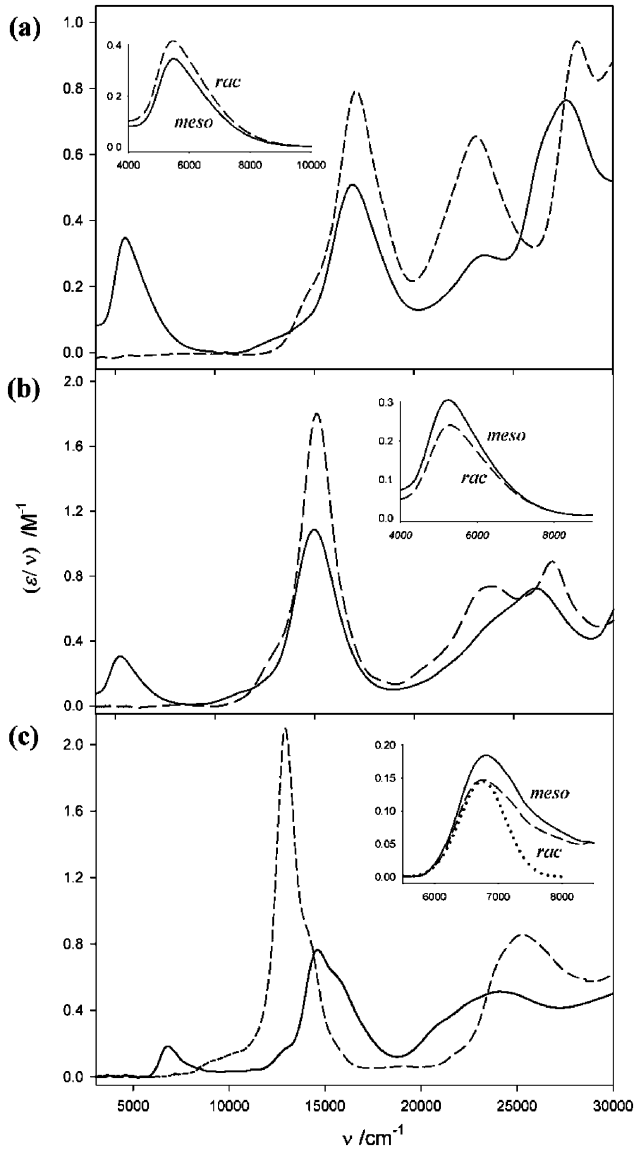

Fig. 5 UV/Vis/NIR spectra of *rac*-$[\{Ru(bpy)_2\}_2(\mu\text{-BL})]^{n+}$ {n = 4 (--), 5 (—)} where BL is (a) 2,5-dpp, (b) dpop or (c) apy, in 0.02 M [(n-$C_4H_9)_4N$]{$B(C_6F_5)_4$}–n-butyronitrile at +25 °C {for BL = 2,5-dpp, dpop} and −35 °C {for BL = apy}. Insets show the overlays of the IVCT bands for the *meso* and *rac* diastereoisomers of each complex. The Gaussian deconvolution of *rac*-$[\{Ru(bpy)_2\}_2(\mu\text{-apy})]^{5+}$ is also shown (···).

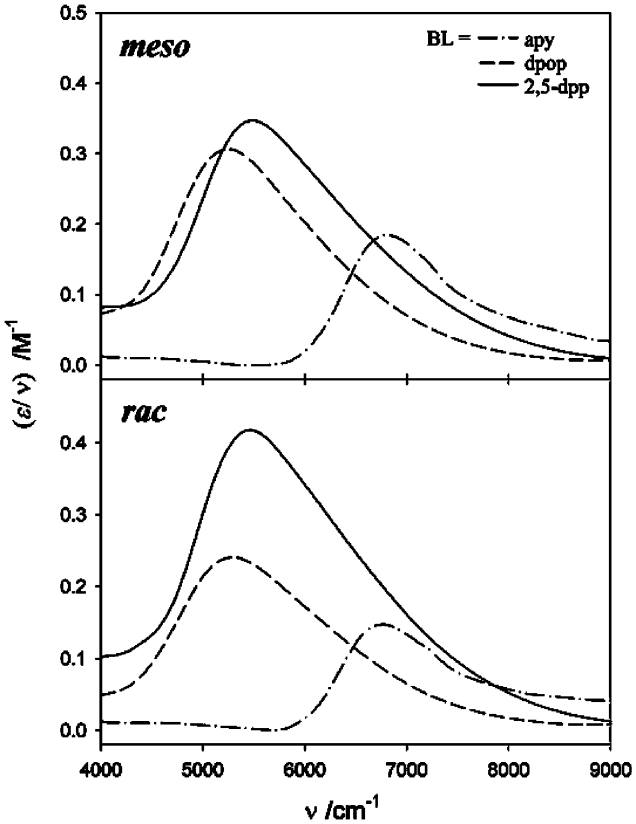

Fig. 6 Overlay of the IVCT bands for the stepped-parallel bridging ligands for *meso*- (a) and *rac*- (b) $[\{Ru(bpy)_2\}_2(\mu\text{-BL})]^{5+}$ in 0.02 M [(n-$C_4H_9)N$]{$B(C_6F_5)_4$}–CH_3CN at +25 °C for BL = 2,5-dpp, dpop and −35 °C for BL = apy.

distinguishing between Classes II (broad, solvent dependent, localised oxidation states) and II–III (narrow, solvent independent, localised oxidation states). In the present case, the weaker solvent dependence of M_1 and the narrower bandwidths for the dpop-bridged diastereoisomers relative to the 2,5-dpp-bridged forms are consistent with a solvent independent (Class II–III) classification in the former case. By comparison, the slight solvent dependence of M_1 for the latter indicates that the systems lie at the borderline between the Class II and Class II–III regimes.

Specific solvation effects are reflected in the plots of the difference between the IVCT parameters for the diastereoisomers {$\Delta\nu_{max}$(*meso*–*rac*), $\Delta\nu_{\frac{1}{2}}$(*meso*–*rac*) and ΔM_1(*meso*–*rac*)} in Fig. S1 (ESI†). Such effects arise due to solvent penetration within the clefts between the terminal bpy rings, as discussed previously for the complexes incorporating linear bridging ligands such as 2,2′-bipyrimidine.[12] The M_1 values for *meso*-$[\{Ru(bpy)_2\}_2(\mu\text{-BL})]^{5+}$ (BL = 2,5-dpp, dpop) are consistently greater than those for the corresponding *rac* forms across the series of solvents. In addition, the magnitude of ΔM_1 varies to a lesser extent for the dpop- relative to the 2,5-dpp-bridged complex, consistent with the greater degree of solvent independence in the former case.

For the 2,5-dpp- and dpop-bridged complexes, the $\Delta\nu_{max}$ and ΔM_1 values increase as the solvent is varied through the series AN, PN, BN, ^{i}BN and BzN for each complex. The magnitudes of these parameters reflect differential solvent interactions with the interior clefts of the diastereoisomeric forms. The largest specific interaction occurs in BzN, as the discrete solvent molecules may be accommodated preferentially within the parallel-shaped interior cleft of the *rac* diastereoisomers of the complexes *i.e.* "below" the plane of the bridging ligand, as shown in Fig. 1 and 4 for the 2,5-dpp- and dpop-bridged forms, respectively.

The dimensions of the interior clefts are reduced for the apy-bridged diastereoisomers (shown in Fig. 8) relative to the 2,5-dpp- and dpop-bridged forms, due to the closer proximity of the metal centres. The interior clefts in the *meso* form are identical "above" and "below" the plane of the bridging

Table 3 IVCT spectral data of the reduced absorption spectra (ε/ν *vs.* ν) for the diastereoisomeric forms of $[\{Ru(bpy)_2\}_2(\mu\text{-BL})]^{5+}$ in 0.02 M $[(n\text{-}C_4H_9)_4N]\{B(C_6F_5)_4\}$–$CH_3CN$ at +25 °C {BL = 2,5-dpp, dpop} and at −35 °C {BL = apy} and parameters derived from the moment analysis of the transitions.[a]

BL	Diastereoisomer	ν_{max} (cm^{-1})	$(\varepsilon/\nu)_{max}$ (M^{-1})	$\Delta\nu_{\frac{1}{2}}$ (cm^{-1})	M_0 (M^{-1})	M_1 (cm^{-1})	$\lvert\mu_{12}\rvert$ (eÅ)	$\Delta\nu_{\frac{1}{2}}^{\circ}$ (cm^{-1})	H_{ab} (cm^{-1})
2,5-dpp	*meso*	5460	0.356	1799	829	5903	0.593	3740	470
	rac	5416	0.428	1861	918	5890	0.624	3725	490
dpop	*meso*	5228	0.315	1665	596	5639	0.503	3660	380
	rac	5268	0.247	1754	488	5717	0.455	3674	347
apy[b]	*meso*	6840	0.243	832	—	—	0.310	3544	432
	rac	6850	0.143	904	—	—	0.234	3546	327

[a] The errors in the observed parameters are ±10 cm^{-1} for ν_{max}, M_1 and $\Delta\nu_{\frac{1}{2}}$, ±0.001 M^{-1} for $(\varepsilon/\nu)_{max}$, ±5 M^{-1} for M_0 and ±0.001 eÅ for $\lvert\mu_{12}\rvert$. [b] $\lvert\mu_{12}\rvert$ determined as $0.0206 \times (\varepsilon_{max}\,\Delta\nu_{\frac{1}{2}}/\nu_{max})^{\frac{1}{2}}$ rather than $0.0206 \times M_0^{\frac{1}{2}}$.

Table 4 IVCT solvatochromism data for the diastereoisomers of $[\{Ru(bpy)_2\}_2(\mu\text{-2,5-dpp})]^{5+}$ in 0.02 M $[(n\text{-}C_4H_9)_4N]\{B(C_6F_5)_4\}$–solvent at +25 °C

		meso					*rac*				
Solvent	$1/D_{op} - 1/D_s$	ν_{max} ±10 (cm^{-1})	$(\varepsilon/\nu)_{max}$ ±0.001 (M^{-1})	$\Delta\nu_{\frac{1}{2}}$ ±10 (cm^{-1})	M_0 (M^{-1})	M_1 (cm^{-1})	ν_{max} ±10 (cm^{-1})	$(\varepsilon/\nu)_{max}$ ±0.001 (M^{-1})	$\Delta\nu_{\frac{1}{2}}$ ±10 (cm^{-1})	M_0 (M^{-1})	M_1 (cm^{-1})
AN	0.5127	5460	0.356	1799	829	5903	5416	0.428	1861	919	5890
PN	0.5011	5434	0.212	1798	572	5878	5400	0.226	1864	380	5860
^{i}BN	0.4795	5486	0.752	1818	792	5931	5464	0.458	1811	835	5885
BN	0.4762	5453	0.518	1766	796	5901	5434	0.260	1786	666	5890
BzN	0.3897	5401	0.341	1675	430	5795	5250	0.166	1842	245	5680

Table 5 IVCT solvatochromism data for the diastereoisomers of $[\{Ru(bpy)_2\}_2(\mu\text{-dpop})]^{5+}$ in 0.02 M $[(n\text{-}C_4H_9)_4N]\{B(C_6F_5)_4\}$–solvent at +25 °C

		meso					*rac*				
Solvent	$1/D_{op} - 1/D_s$	ν_{max} ±10 (cm^{-1})	$(\varepsilon/\nu)_{max}$ ±0.001 (M^{-1})	$\Delta\nu_{\frac{1}{2}}$ ±10 (cm^{-1})	M_0 (M^{-1})	M_1 (cm^{-1})	ν_{max} ±10 (cm^{-1})	$(\varepsilon/\nu)_{max}$ ±0.001 (M^{-1})	$\Delta\nu_{\frac{1}{2}}$ ±10 (cm^{-1})	M_0 (M^{-1})	M_1 (cm^{-1})
AN	0.5127	5228	0.315	1665	596	5639	5268	0.247	1754	488	5717
PN	0.5011	5213	0.286	1607	530	5612	5250	0.204	1686	390	5713
^{i}BN	0.4795	5223	0.331	1575	606	5617	5223	0.118	1659	220	5738
BN	0.4762	5206	0.213	1591	375	5608	5268	0.230	1654	425	5712
BzN	0.3897	5144	0.275	1502	472	5559	5208	0.152	1544	274	5711

Table 6 IVCT solvatochromism data for the diastereoisomers of $[\{Ru(bpy)_2\}_2(\mu\text{-apy})]^{5+}$ in 0.02 M $[(n\text{-}C_4H_9)_4N]\{B(C_6F_5)_4\}$–solvent at −35 °C

		meso			*rac*		
Solvent	$1/D_{op} - 1/D_s$	ν_{max} ±10 (cm^{-1})	$(\varepsilon/\nu)_{max}$ ±0.001 (M^{-1})	$\Delta\nu_{\frac{1}{2}}$ ±10 (cm^{-1})	ν_{max} ±10 (cm^{-1})	$(\varepsilon/\nu)_{max}$ ±0.001 (M^{-1})	$\Delta\nu_{\frac{1}{2}}$ ±10 (cm^{-1})
AN	0.5127	6840	0.243	832	6850	0.143	904
PN	0.5011	6790	0.121	778	6780	0.147	810
^{i}BN	0.4795	6830	0.178	823	6760	0.180	850
BN	0.4762	6800	0.183	885	6760	0.147	847

Table 7 Summary of the solvent dependence of ν_{max} for $[\{Ru(bpy)_2\}_2(\mu\text{-BL})]^{5+}$ {BL = 2,5-dpp, dpop, apy} according to the dielectric continuum model

Complex	Slope $e^2(1/a - 1/d)$ (cm^{-1})	Intercept $\lambda_i + \Delta E' + \Delta E_0$ (cm^{-1})	R^2
meso-$[\{Ru(bpy)_2\}_2(\mu\text{-2,5-dpp})]^{5+}$	455 ± 270	5232 ± 130	0.48
rac-$[\{Ru(bpy)_2\}_2(\mu\text{-2,5-dpp})]^{5+}$	1455 ± 530	4706 ± 250	0.71
meso-$[\{Ru(bpy)_2\}_2(\mu\text{-dpop})]^{5+}$	676 ± 109	4884 ± 5	0.93
rac-$[\{Ru(bpy)_2\}_2(\mu\text{-dpop})]^{5+}$	440 ± 200	5039 ± 10	0.60
meso-$[\{Ru(bpy)_2\}_2(\mu\text{-apy})]^{5+}$	369 ± 925	6633 ± 455	0.07
rac-$[\{Ru(bpy)_2\}_2(\mu\text{-apy})]^{5+}$	2185 ± 770	5712 ± 380	0.80

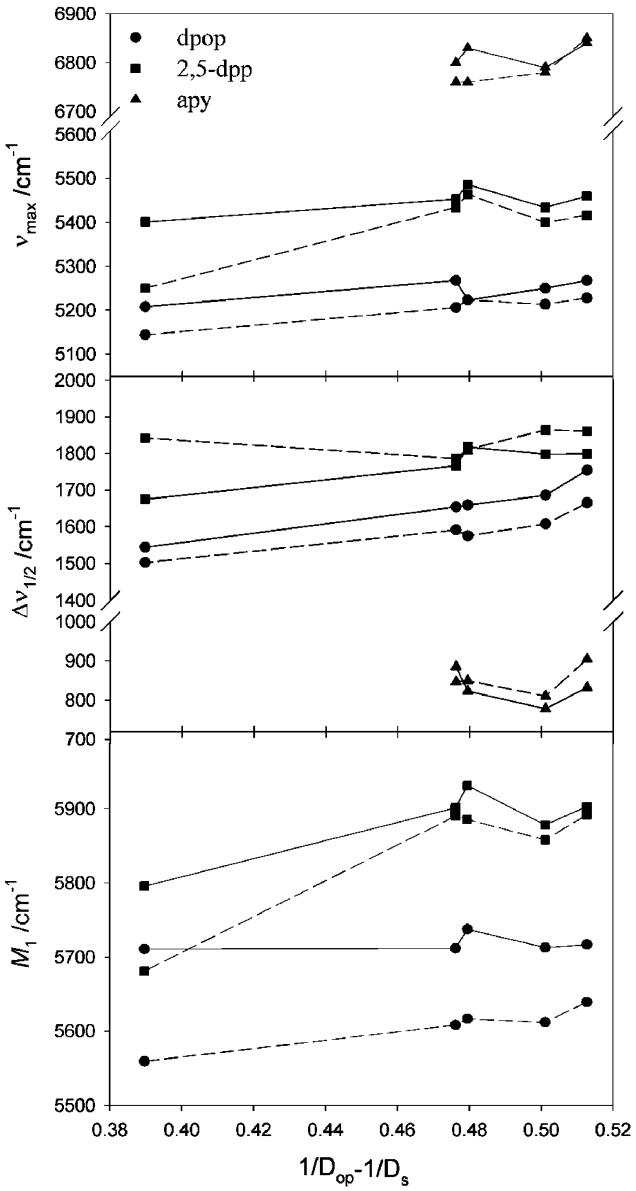

Fig. 7 Solvent dependence of ν_{max}, $\Delta\nu_{\frac{1}{2}}$ and M_1 for the *meso* (—) and *rac* (--) diastereoisomers of $[\{Ru(bpy)_2\}_2(\mu\text{-BL})]^{5+}$ in 0.02 M $[(n\text{-}C_4H_9)N]\{B(C_6F_5)_4\}$–solvent at +25 °C for BL = 2,5-dpp, dpop and −35 °C for BL = apy. Error bars are omitted for clarity.

ligand and are more ideally disposed to accommodate aliphatic solvent molecules compared with the *rac* form. In the latter, the dimensions of the interior clefts differ on either side of the bridging ligand plane. The different dimensionalities of the clefts between the diastereoisomeric forms would account for the increase in $\Delta\nu_{max}$(*meso*–*rac*) as the size of the aliphatic nitrile solvent is increased through the series AN, PN, BN and ^{i}BN.

A recent IVCT solvatochromism study on the diastereoisomeric forms of $[\{Ru(bpy)_2\}_2(\mu\text{-bpm})]^{5+}$ (shown in Fig. S2, ESI†) in the series of nitrile solvents investigated here found a marked specific solvent effect in acetonitrile due to penetration of the relatively small solvent molecules between the interior clefts.[12] The absence of this specific interaction in acetonitrile

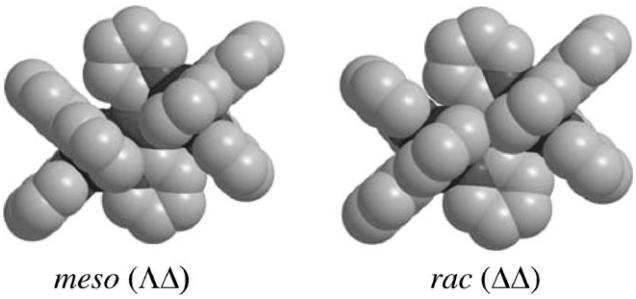

Fig. 8 Chem3D™ representations[52] (view from above the plane of the bridging ligand) of the *meso* (ΛΔ) and *rac* (ΔΔ) diastereoisomers of $[\{Ru(bpy)_2\}_2(\mu\text{-apy})]^{4+}$.

for the stepped-parallel complexes demonstrates that the dimensionalities of the interior clefts in the diastereoisomers of a linear complex are more appropriate to accommodate the small acetonitrile molecules.

Conclusions

The synthesis and separation of the diastereoisomeric forms of the complexes $[\{Ru(bpy)_2\}_2(\mu\text{-BL})]^{4+}$ based on the series of "stepped-parallel" bridging ligands 2,5-dpp, dpop and apy are reported. Electrochemical and intervalence charge transfer (IVCT) studies on the complexes reveal a high degree of metal–metal interaction, which is consistent with a Class II–III classification for the systems. IVCT solvatochromism studies on the diastereoisomers of $[\{Ru(bpy)_2\}_2(\mu\text{-BL})]^{5+}$ (BL = 2,5-dpp, dpop and apy) reveal that the systems are independent of solvent.

The series of complexes have been investigated extensively over the past two decades as the basis of novel molecular materials capable of performing useful light- and/or redox-induced functions.[47–51] While these studies were performed without regard for the inherent stereochemistry of the systems, the present work further supports our recent findings[12–14] which demonstrate that stereochemical influences provide a significant contribution to the barrier to intramolecular electron transfer, and are indeed manifested in the electrochemical, spectral and IVCT properties of the systems. The realisation that metal–metal interactions in dinuclear polypyridyl complexes can be modified by the variation of their stereochemical properties has significant consequences for controlling such interactions in higher nuclearity polymetallic assemblies.

Acknowledgements

We gratefully acknowledge Prof. Tom Meyer and Dr Dana Dattelbaum (Los Alamos National Laboratory, USA) for supplying the complex $[\{Ru(bpy)_2\}_2(\mu\text{-dpop})](PF_6)_4$ for these studies. This work was supported by the Australian Research Council.

References

1 N. S. Hush, *Prog. Inorg. Chem.*, 1967, **8**, 391–444.
2 N. S. Hush, *Electrochim. Acta*, 1968, **13**, 1005–1023.
3 C. Creutz, *Prog. Inorg. Chem.*, 1983, **30**, 1–73.

4 R. J. Crutchley, *Adv. Inorg. Chem.*, 1994, **41**, 273–325.
5 K. Kalyanasundaram and M. K. Nazeeruddin, *Inorg. Chim. Acta*, 1994, **226**, 213–230.
6 M. D. Ward, *Chem. Soc. Rev.*, 1995, **24**, 121–134.
7 K. D. Demadis, C. M. Hartshorn and T. J. Meyer, *Chem. Rev.*, 2001, **101**, 2655–2685.
8 L. S. Kelso, D. A. Reitsma and F. R. Keene, *Inorg. Chem.*, 1996, **35**, 5144–5153.
9 T. J. Rutherford and F. R. Keene, *Inorg. Chem.*, 1997, **36**, 2872–2878.
10 T. J. Rutherford, O. Van Gijte, A. Kirsch-De Mesmaeker and F. R. Keene, *Inorg. Chem.*, 1997, **36**, 4465–4474.
11 J. A. Treadway, P. Chen, T. J. Rutherford, F. R. Keene and T. J. Meyer, *J. Phys. Chem. A*, 1997, **101**, 6824–6826.
12 D. M. D'Alessandro and F. R. Keene, *Chem. Phys.*, 2006, DOI: 10.1016/j.chemphys.2005.09.016.
13 D. M. D'Alessandro, L. S. Kelso and F. R. Keene, *Inorg. Chem.*, 2001, **40**, 6841–6844.
14 D. M. D'Alessandro, P. C. Junk and F. R. Keene, *Supramol. Chem.*, 2005, **17**, 529–542.
15 F. R. Keene, *Chem. Soc. Rev.*, 1998, **27**, 185–193.
16 F. R. Keene, *Coord. Chem. Rev.*, 1997, **166**, 122–159.
17 D. M. D'Alessandro and F. R. Keene, *Dalton Trans.*, 2006, DOI: 10.1039/b512625h.
18 D. M. D'Alessandro, M. S. Davies and F. R. Keene, *Inorg. Chem.*, 2006, DOI: 10.1021/ic051699i.
19 S. Ernst, V. Kasack and W. Kaim, *Inorg. Chem.*, 1988, **27**, 1146–1148.
20 S. D. Ernst and W. Kaim, *Inorg. Chem.*, 1989, **28**, 1520–1528.
21 W. Kaim and S. Kohlmann, *Inorg. Chem.*, 1987, **26**, 68–77.
22 G. Giuffrida and S. Campagna, *Coord. Chem. Rev.*, 1994, **135**, 517–531.
23 G. Denti, S. Campagna, L. Sabatino, S. Serroni, M. Ciano and V. Balzani, *Inorg. Chem.*, 1990, **29**, 4750–4758.
24 J. E. B. Johnson and R. R. Ruminski, *Inorg. Chim. Acta*, 1993, **208**, 231–237.
25 J. A. Treadway, G. F. Strouse, R. R. Ruminski and T. J. Meyer, *Inorg. Chem.*, 2001, **40**, 4508–4509.
26 B. D. Yeomans, L. S. Kelso, P. A. Tregloan and F. R. Keene, *Eur. J. Inorg. Chem.*, 2001, 239–246.
27 L. S. Kelso, PhD Thesis, James Cook University, Townsville, Queensland, Australia, 2000.
28 R. LeSuer and W. E. Geiger, *Angew. Chem., Int. Ed.*, 2000, **39**, 248–250.
29 B. T. Patterson and F. R. Keene, *Inorg. Chem.*, 1998, **37**, 645–650.
30 C. M. Duff and G. A. Heath, *Inorg. Chem.*, 1991, **30**, 2528–2535.
31 D. M. D'Alessandro and F. R. Keene, *Chem.–Eur.J.*, 2005, **11**, 3679–3688.
32 J. R. Reimers and N. S. Hush, *Inorg. Chem.*, 1990, **29**, 3686–3697.
33 N. C. Fletcher, P. C. Junk, D. A. Reitsma and F. R. Keene, *J. Chem. Soc., Dalton Trans.*, 1998, 133–138.
34 T. Togano, N. Nagao, M. Tsuchida, H. Kumakura, K. Hisamatsu, F. S. Howell and M. Mukaida, *Inorg. Chim. Acta*, 1992, **195**, 221–225.
35 X. Hua, PhD Thesis, University of Fribourg, Fribourg, Switzerland, 1993.
36 N. C. Fletcher and F. R. Keene, *J. Chem. Soc., Dalton Trans.*, 1999, 683–689.
37 S. M. Molnar, K. R. Neville, G. E. Jensen and K. J. Brewer, *Inorg. Chim. Acta*, 1993, **206**, 69–76.
38 E. C. Constable and J. Lewis, *Inorg. Chim. Acta*, 1983, **70**, 251–253.
39 A. Juris, S. Barigelletti, S. Campagna, V. Balzani, P. Belser and A. von Zelewsky, *Coord. Chem. Rev.*, 1988, **84**, 85–277.
40 M. Marcaccio, F. Paolucci, C. Paradisi, S. Roffia, C. Fontanesi, L. J. Yellowlees, S. Serroni, S. Campagna, G. Denti and V. Balzani, *J. Am. Chem. Soc.*, 1999, **121**, 10081–10091.
41 D. M. D'Alessandro and F. R. Keene, *Dalton Trans.*, 2004, 3950–3954.
42 K. A. Goldsby and T. J. Meyer, *Inorg. Chem.*, 1984, **23**, 3002–3010.
43 D. E. Richardson and H. Taube, *J. Am. Chem. Soc.*, 1983, **105**, 40–51.
44 C. Creutz, M. D. Newton and N. Sutin, *J. Photochem. Photobiol., A*, 1994, **82**, 47–59.
45 R. J. Cave and M. D. Newton, *Chem. Phys. Lett.*, 1996, **249**, 15–19.
46 N. S. Hush, *Coord. Chem. Rev.*, 1985, **64**, 135–157.
47 C. G. Garcia, J. F. de Lima and N. Y. M. Iha, *Coord. Chem. Rev.*, 2000, **196**, 219–247.
48 P. Belser, S. Bernhard, C. Blum, A. Beyeler, L. De Cola and V. Balzani, *Coord. Chem. Rev.*, 1999, **190–192**, 155–169.
49 V. Balzani, A. Juris, M. Venturi, S. Campagna and S. Serroni, *Chem. Rev.*, 1996, **96**, 759–833.
50 P. Belser, R. Dux, M. Baak, L. De Cola and V. Balzani, *Angew. Chem., Int. Ed. Engl.*, 1995, **34**, 595–598.
51 V. Balzani and F. Scandola, *Supramolecular Photochemistry*, Ellis Horwood, Chichester, 1991.
52 *Chem3D Ultra v. 8.0*, Cambridge Soft Corporation, Cambridge, MA 02140, USA, 2003.
53 *Varian WinUV v. 2.00(25)*, Varian Australia Pty. Ltd., Melbourne, Australia, 1999.